www.czasopisma.pan.pl PAN POLSKA AKADEMIA NAUK www.journals.pan.pl

Arch. Metall. Mater. **65** (2020), 1, 117-124

DOI: 10.24425/amm.2019.131104

R. FILIPEK[1*], K. SZYSZKIEWICZ-WARZECHA[1], J. SZCZUDŁO[1]

CORROSION OF STEEL IN CONCRETE – MODELING OF ELECTROCHEMICAL POTENTIAL MEASUREMENT IN 3D GEOMETRY

The paper presents a 3D model and simulations of corroding reinforcement bars in a concrete element. Electric potential distributions are calculated in the concrete matrix and on its surface for two rebars arrangements with one or three active (anodic) sites to assess the reliability and identify possible problems when standard test measurements for corrosion assessment in concrete structures are used and conclusion on the corrosion state is inferred. The values of the potential strongly depend on a concrete layer thickness and beyond the threshold of 5-7 cm it is hardly possible to detect the number of active sites on the rebar. Also conductivity – which is not constant in real world constructions – is an important factor. Thus without estimation of the state of concrete it is difficult to draw reliable conclusions on the corroding activity from shear potential measurements on the surface.

Keywords: Reinforced concrete corrosion, 3D modeling, non-destructive testing

1. Introduction

Corrosion of steel embedded in concrete structures is one of the most important degradative processes which affect such structures leading to their premature loss of serviceability, need of costly repairing or renovating, and even to structural collapse. Its economic consequences are considerable and some sources estimate that for civil engineering structures made of reinforced concrete, corrosion accounts for about 80% of observed pathologies [1]. Since the degradation of reinforced concrete structure is strongly related to the corrosion of embedded steel rebars, the assessment of this process is highly significant for the proper safety management.

To assess the possibility of estimating the corrosion activity in a construction element by measurements as are postulated in the relevant standards (protocols) and also to identify the potential pitfalls and ambiguities resulting from such measurements, we have performed a series of parametric simulations with different length and number of anodic sites, with varying the thickness of the concrete layer above the rebars, equilibrium potentials, exchange current densities, and using two types of rebars arrangements – one row and two rows. However, as this work is not intended to cover the subject in its full extent but only to hint at the problems with such protocols and to direct attention at the computational tools, in what follows we present only part of these results. Similar models have been used recently [2,3] although the authors applied in the kinetic expressions only one part of the Butler-Volmer expression (*cf.* equation (8)).

2. Mechanisms of rebar corrosion protection in concrete

The most important constituent of concrete is the hydraulic binder (cement) which before hydration consists mainly of four minerals: tricalcium silicate ($3CaO{\cdot}SiO_2$), dicalcium silicate ($2CaO{\cdot}SiO_2$), tricalcium aluminate ($3CaO{\cdot}Al_2O_3$), and tetracalcium alumino-ferrite ($4CaO{\cdot}Al_2O_3{\cdot}Fe_2O_3$). On mixing it with water these minerals undergo a complex series of reactions which after several stages transform the paste into a hardened matrix of hydrated products. The development of physical structure and mechanical properties are primarily dictated by the reactions involving[1] C_3S and C_2S which produce a C-S-H gel (of ill-defined composition and structure) and calcium hydroxide (in the form of portlandite crystals). From the point of view of the corrosion behavior of steel in concrete it is fundamental that the aqueous phase present in the pores of hardened cement acquires

[1] In cement chemistry notation: C = CaO, S = SiO_2, C_3S = $3CaO{\cdot}SiO_2$, C_2S = $2CaO{\cdot}SiO_2$.

[1] AGH UNIVERISTY OF SCIENCE AND TECHNOLOGY, FACULTY OF MATERIALS SCIENCE AND CERAMICS, AL. MICKIEWICZA 30, 30-059 KRAKÓW, POLAND

* Corresponding author: rof@agh.edu.pl

a high pH value. Initially this phase contains mainly hydroxides and sulfates of calcium, sodium, and potassium. Thus, after an initial period of hydration, the cement paste acquires pH values in excess of 13, and this alkaline environment provides the primary mechanism of corrosion protection in concrete resulting from the inhibitive nature of hydroxyl ions.

The electrochemical theory holds that the metal corrosion phenomena are the combination of an anodic oxidation (metal dissolution), a cathodic reduction (typically involving oxygen molecules or hydrogen ions), and the electrical coupling of these reactions by the flow of electrons from anode to cathode in the metal phase [4]. However, it should be appreciated that corrosion phenomena also involve other than oxidation-reduction reactions such as acid-base reactions and transport processes. For example, the metal ions produced in the surface oxidation move into the aqueous solution to form hydrated metal ions or other metal-ion complexes which are typical Lewis acid-base reactions. Furthermore, in order to sustain the anodic dissolution process by its reduction counterpart, the constant supply of substrate species must occur usually by the diffusion, migration, or convection modes of transport in the electrolyte phase.

In principle, the anodic and cathodic reactions can take place either statistically distributed all over the surface of the rebar steel or be separated at specific cathodic and anodic zones. The first case gives rise to the uniform corrosion while the second – the localized corrosion. According to the different relative spatial locations of anodic and cathodic zones, the corrosion of steel rebars in concrete are classified as *microcell* and *macrocell* corrosion systems. Microcell corrosion consists of pairs of immediately adjacent anodes and cathodes, and the anodic reaction is totally supported by the local cathodic reaction. On the other hand, macrocell corrosion consists of spatially isolated anodes and cathodes, and the anodic reaction in the active zone is supported by the cathodic reaction in the passive zone [5].

It is generally accepted that in the case of carbon steel corrosion, fundamentally, the anodic and cathodic reactions in an oxygenated aqueous environment are the oxidation of iron and the reduction of dissolved oxygen, summarized as follows [6]:

$$Fe \rightarrow Fe^{2+}(aq) + 2e^{-} \tag{1}$$

$$O_2 + 2H_2O + 4e^{-} \rightarrow 4OH^{-}(aq) \tag{2}$$

Moreover, in the anodic region, ferrous iron will react with hydroxyl groups and produce hydroxide which in turn oxidized further into ferric iron:

$$Fe^{2+} + 2OH^{-} \rightarrow Fe(OH)_2 \tag{3}$$

$$4Fe(OH)_2 + O_2 + 2H_2O \rightarrow 4Fe(OH)_3 \tag{4}$$

As was pointed above, concrete normally provides a high degree of protection to the reinforcing bars against corrosion due to the high alkalinity (pH > 13.5) of the pore solution which develops a passivity layer on its surface. But when sufficient chloride ions penetrate through the concrete cover and reach the surface of the rebar or when the pH value of the pore solution falls due to carbonation, the protective film is destroyed and the steel becomes depassivated.

Chloride-induced depassivation: The mechanism by which chloride ions break down the passive film is still not fully understood. It is obvious that this mechanism is related to the passivation process itself and the structure of the passive film which can be divided into two types (*crystalline oxide models* and *hydrated polymeric oxide models*). For instance, [7] identified and analyzed six possible break down mechanisms. One of the hypotheses holds that the chloride ions become incorporated into passive film and reduce its resistance. This incorporation is not uniform and, where it occurs, it allows a more rapid reaction and the establishment of an anodic area where corrosion continues while the remaining steel stays passive. A second hypothesis holds the chloride ions compete with the hydroxyl ions (OH^{-}) for combining with Fe^{2+} cations, and because the Cl^{-} ions form highly soluble complexes with the Fe^{2+} ions (mainly, $[FeCl_4]^{2-}$), a passive film is not formed and the process stimulates further metal dissolution. The soluble iron chloride complexes diffuse away from the surface and subsequently break down resulting in the formation of expansive corrosion products and, simultaneously freeing the Cl^{-} ions, which can migrate back to the steel and react again. In this overall process, hydroxyl ions are continuously consumed, locally decreasing the pH and thus enhancing metal dissolution. As the Cl^{-} ions are not consumed this type of reaction becomes an autocatalytic process [8].

Carbonation induced depassivation: Carbon dioxide from the atmosphere reacts with the calcium hydroxide and other hydroxides in the cement/concrete paste by the following reaction [9]

$$Ca(OH)_2 + CO_2 \rightarrow CaCO_3 + H_2O \tag{5}$$

effectively neutralizing the pore solution. The depth of carbonation increases with time and the rate it moves is a function of relative humidity (it is most rapid in the 50%-70% RH range). When the carbonation front reaches the reinforcement, the passive film is no longer stable and active corrosion may start. Unlike the chloride-induced corrosion, this corrosion is relatively homogeneous. Moreover, the corrosion products tend to be more soluble (in the neutral carbonated concrete) and may diffuse to the surface appearing as rust stains on the concrete, rather than precipitating in the concrete cover and causing stresses and cracking.

Although intermediate RH provides the highest rate of carbonation, active corrosion of any significance does not occur in that range. Consequently, the most aggressive environment for carbonation-induced corrosion is alternate semi-dry and wet cycles. Carbonation can thus be a major factor in hot climates where the concrete is easily dried out and periodically subjected to rainstorms. Chloride attack and carbonation can act synergistically and are responsible for major problems in coastal areas.

3. Measurements and standards

The electric potential measurement is one of the techniques used for detecting and locating active corrosion zones in reinforced concrete structures. It is based on the electrochemical principles and involves a reference electrode and a high impedance voltmeter as measuring devices. The basic idea is to identify the gradients of potentials on the surface of a concrete structure which are generated by the existing anodic and cathodic active areas on the rebars surface. During the measurement the reference electrode is connected to the COM(–) terminal of the voltmeter while the reinforcing steel to the (+) terminal and the electrode is moved to different positions over the surface. A wet sponge can be used to ensure a good electrical contact between the electrode and the concrete surface. To facilitate an easy plot of the potential map the measurement should be performed at points of a regular grid. The most frequently used reference electrode in field measurements is the saturated copper electrode $Cu(s)/CuSO_4(aq, sat)$ with potential 0.316 V (vs. SHE). In laboratory, however, another electrode is conveniently used, namely the saturated calomel electrode (SCE) with potential 0.244 V (vs. SHE) [10].

In order to normalized such tests and allow reliable comparisons several standards have been published. Here we mention two important documents:

(i) The American standard ASTM C876-09 ('*Standard Test Method for Corrosion Potentials of Uncoated Reinforcing Steel in Concrete*').

(ii) The European recommendation RILEM TC 154-EMC ('*Electrochemical Techniques for Measuring Metallic Corrosion*').

Both standards define the apparatus to be used, protocol for the implementation of *in situ* measurements, the methods of interpretation, evaluation of a possible corrosion current, and reporting. Fundamentally, both standards are based on the assumption that under some conditions the knowledge of the electric potential distribution over the surface of the concrete element may supply information about the distribution of the electric currents inside the element and in consequence can be used to infer the state of corrosion activity on the reinforcing bars. Although such approach is reasonable and can be fruitful in many circumstances, we would like to point out in the present paper some of its pitfalls and limitations:

1) Problem with the localization of anodic zones and confinement of the polarization current (guard-ring electrodes). Especially, comparison between the distribution of the guard and polarization currents and the distribution assumed in the standard.
2) Absence of the natural galvanic current exchanged between the active and passive sites.
3) How the potential on the surface of the concrete element depends on the distance to the rebars and their geometrical arrangement.

4. Mathematical model

The calculation of the current distribution for the investigated problem requires a solution of Laplace's equation with nonlinear boundary conditions. Let Φ be the electric potential as a function of position. In a linear medium, the current density is given by [9]

$$\mathbf{j} = -\sigma \nabla \Phi \tag{6}$$

where σ is the electric conductivity of the concrete. The equation of electric charge conservation requires $\operatorname{div} \mathbf{j} = 0$, which after substituting to equation (6) leads to

$$\operatorname{div}(-\sigma \nabla \Phi) = 0 \tag{7}$$

Mathematically, the boundary conditions in this problem are of the Neumann type. On the parts of the boundary where no reactions take place we assume insulation (zero normal component of the current density), but on the parts where reactions operate some kinetics must be involved. Despite the fact that both the anodic dissolution and cathodic reduction described by equations (1) and (2) are in fact quite complicated (in terms of the full kinetics mechanism) it is commonly accepted that the Butler-Volmer equation gives satisfactory results (at least as the current distribution in bulk and on the surface are concerned). Therefore we will use the following boundary conditions [11]:

$$\begin{aligned}
&\mathbf{j}\cdot\boldsymbol{n} = j_a^0\left(e^{2.3(\Phi-\Phi_a^0)/\beta_{a,a}} - e^{-2.3(\Phi-\Phi_a^0)/\beta_{c,a}}\right) \ (\textit{anodic zone}),\\
&\mathbf{j}\cdot\boldsymbol{n} = j_c^0\left(e^{2.3(\Phi-\Phi_c^0)/\beta_{a,p}} - e^{-2.3(\Phi-\Phi_c^0)/\beta_{c,p}}\right) \ (\textit{catodic zone}),\\
&\mathbf{j}\cdot\boldsymbol{n} = 0 \quad (\textit{no reaction, insulating part}),
\end{aligned} \tag{8}$$

where $j_{a/c}^0$ is the anodic (cathodic) exchange current density, $\Phi_{a/c}^0$ is the anodic (cathodic) reaction equilibrium potential, $\beta_{a/c}$ is the anodic (cathodic) Tafel slope, and $\boldsymbol{n}$ is the normal (outer) vector on the boundary. In writing equations we adopted the convention recommended by IUPAC that an anodic current is positive while a cathodic current is negative. No concentration

TABLE 1

Physical parameters used for numerical simulations

Parameter	Value
Anodic exchange current density, j_a^0 (A/m^2)	10^{-1}
Cathodic exchange current density, j_c^0 (A/m^2)	10^{-4}
Anodic equilibrium potential, Φ_a^0 (V vs.SHE)	–0.7
Cathodic equilibrium potential, Φ_c^0 (V vs.SHE)	–0.1
Tafel slope for anodic direction of reaction at active zone, $\beta_{a,a}$ (V)	0.06
Tafel slope for cathodic direction of reaction at active zone, $\beta_{c,a}$ (V)	0.16
Tafel slope for anodic direction of reaction at passive zone, $\beta_{a,p}$ (V)	0.4
Tafel slope for cathodic direction of reaction at passive zone, $\beta_{c,p}$ (V)	0.16
Electrical conductivity, σ (S/m)	0.02, 0.002, 0.0002

polarization is used in (8) because we do not consider here the mass transfer effects. The model presented above in the form of equations (6)-(8) is in the electrochemistry literature usually referred to as the *secondary current and potential distribution*.

TABLE 2

Geometrical parameters used for numerical simulations

Parameter	Value (cm)
Length of the box, L	50
Height of the box	$(3/2) \cdot d_{b,rb} + 2 \cdot d_{rebar} + d_{cover}$
Depth of the box	$3 \cdot d_{br} + 3 \cdot d_r$
Length of the anodic zone, L_{anode}	0.1, 0.5, 1.0, 1.5, 2.0
Depth of the concrete cover, d_{cover}	1, 2.5, 5, 7.5, 10
Diameter of the cylindrical rebars, d_{rebar}	1
Distance between rebars, $d_{b,rb}$	10

5. Numerical study

The model presented by Eqs. (6), (7), and (8) allows carrying out the quantitative numerical computations of the electric current and electric potential behavior in a system similar to a real-world concrete construction element with steel rebars under the assumption that corrosion process of the macrocell type is active on the surface of the middle rebar in the upper row (see Fig. 1). In Table 1 and Table 2 we list the physical and geometrical parameters, respectively, used in the model. To solve these equations the finite elements method (FEM) has been used as is now common in electrochemical simulations when 2D or 3D geometry is involved. The details of this method can be found elsewhere, and we particularly recommend [12].

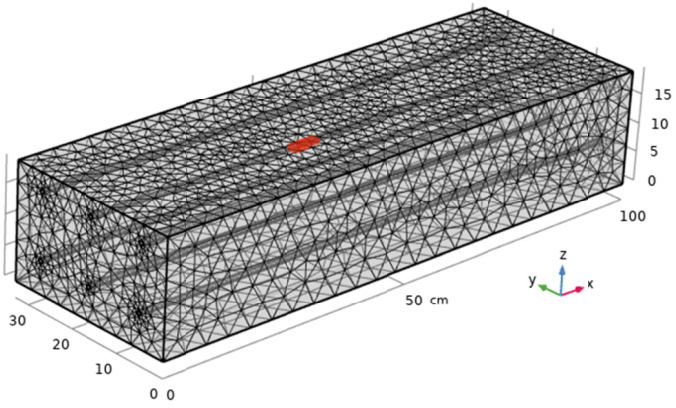

Fig. 1. Geometrical model and meshing. The structural element has the form of a box with two rows of steel bars. The middle bar of the upper of contains an active anodic site (red color)

Fig. 2 presents typical results of the electric potential distribution on the top part of the concrete element containing one row of rebars when the middle rebar has an active corrosion site. The rest of the surfaces of the bars are passive (cathodic) electrode where the oxygen reduction takes place.

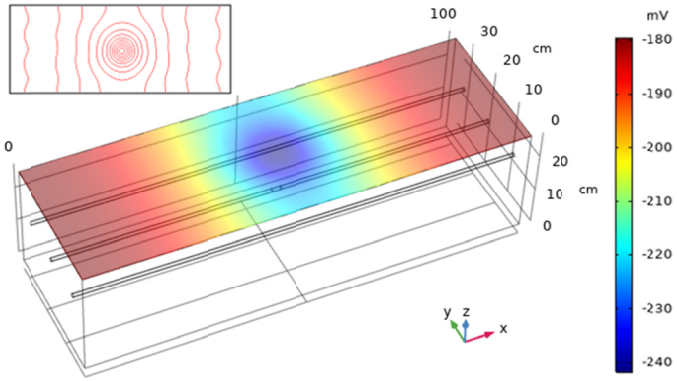

Fig. 2. Distribution of electric potential on the top cover of a reinforced concrete element with two rows of steel bars embedded inside the element. The middle bar of the first row has an active anodic side of length 1 cm. The inset shows the isolines of the potential distribution

In Fig. 3, the electric potential inside the concrete matrix of the element is shown. For better insight it is presented only on a selected cross-section.

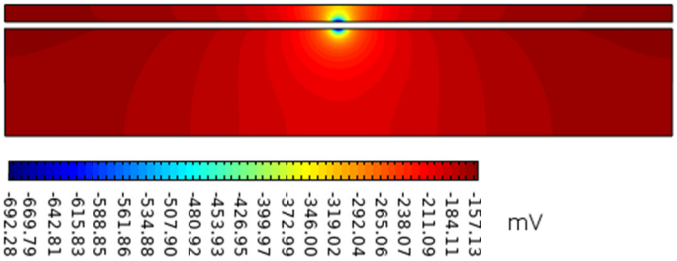

Fig. 3. Plot of the electric current potential on the cross-section through the sample. The cutting plane is parallel to the coordinate system plane XZ and is placed at Y the position such that it goes along the axis of the middle rebar

On the other hand, Fig. 4 displays the same potential in the form of a function along the line which is on the top of the cylindrical rebar with the active (anodic) site. As is expected, the potential dramatically drops in the active region. It is due to the fact that the plots we present show the electric potential Φ in the electrolyte phase (concrete matrix) while the potential of the metallic rebars is everywhere constant, so the drop means

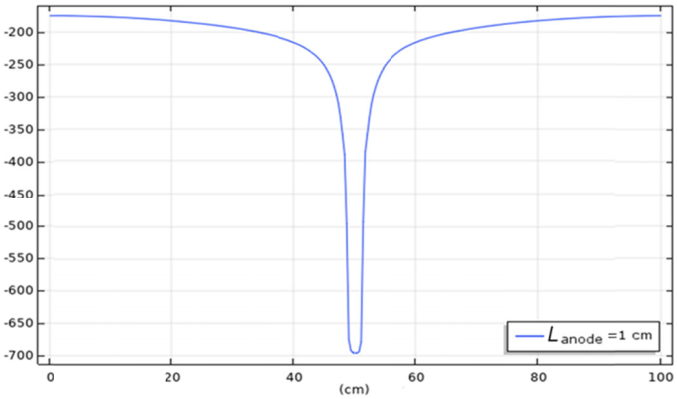

Fig. 4. Plot of the electric potential on the line going along the surface of the middle rebar with the active (anodic) site

that the relative surface potential is more positive as is expected for the anodic site.

In Fig. 5 three plots of the electric potential on the top surface are compared. It is one row arrangement of equipotential rebars with one active site on the middle bar (see Fig. 1). Although in each case there is a visible variation of potential, its relative change over the surface is decreasing as the thickness of the cover grows. It is rather obvious that in the third case (right panel, 10 cm) the differences are so small that practically it is not feasibly to detect them with standard equipment used during *in situ* measurements.

Fig. 6 shows results of the same type of calculations but for different size of the active site on the middle rebar (ten time longer than in Fig. 5). The trend is the same as previously but the values of the potential more negative. This confirms the expected outcome that greater anodic site generate bigger (absolute values) potentials (while all other parameters are kept the same).

Fig. 8 demonstrates potential distribution along the line on the surface of the middle rebar (with active site) for three cover thicknesses (1, 5, 10 cm) and two sizes of active site (1 and 2 cm). It is readily visible an abrupt fall of the potential, but it must be borne in mind that this effect is deep inside the sample to which the standard protocol has no access.

Fig. 9 shows analogous potential distribution (along the line on the surface of the middle rebar) but this time in two rows arrangement. The qualitative behavior is similar as in the one row case although the ranges of electric potential are different.

In a real world context we can expect that corroding rebar develops in fact more than one active macrocell anodic site. To assess the influence of such situation on the electric potential measured on the external part of the construction element we present a model with *three anodic sites* (Fig. 10**)**.

Fig. 11 summarizes the results of computation of electric potential and its behavior when three active site are present. As

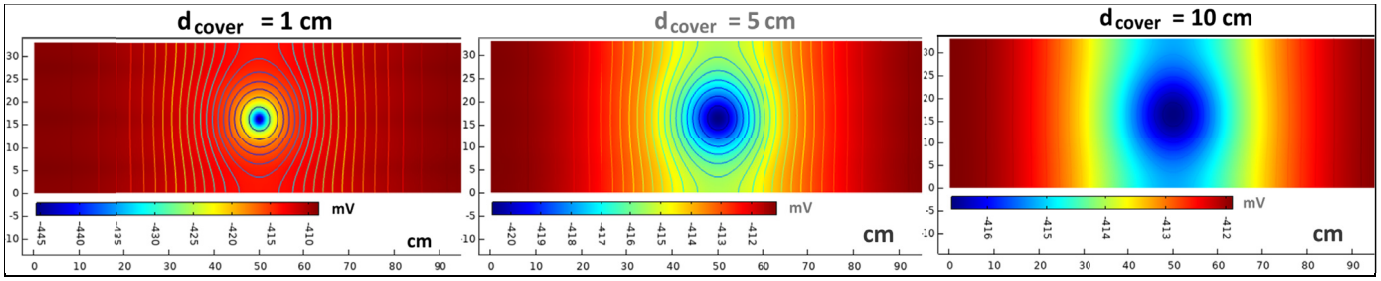

Fig. 5. One row of rebars. Color maps and isolines of electric potential on the top surface of the construction element and its dependence on the thickness of the layer. Length of the active site L_{anode} = 0.1 cm. Potential ranges (in mV): [–445, –410] (left panel – 1 cm thickness), [–420, –410] (middle panel – 5 cm thickness), and [–416, –412] (right panel – 10 cm thickness)

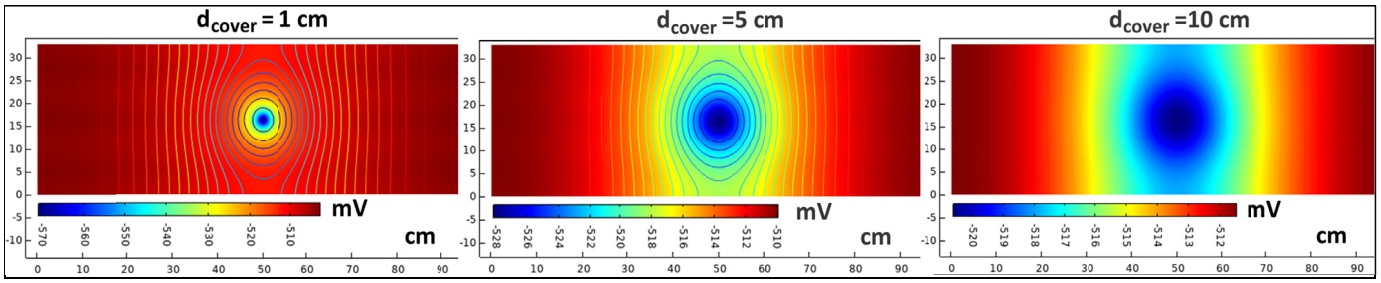

Fig. 6. One row of rebars. Color maps and isolines of electric potential on the top surface of the construction element and its dependence on the thickness of the layer. Length of the active site L_{anode} = 1 cm. Potential ranges (in mV): [–570, –515] (left panel – 1 cm thickness), [–528, –510] (middle panel – 5 cm thickness), and [–520, –510] (right panel – 10 cm thickness)

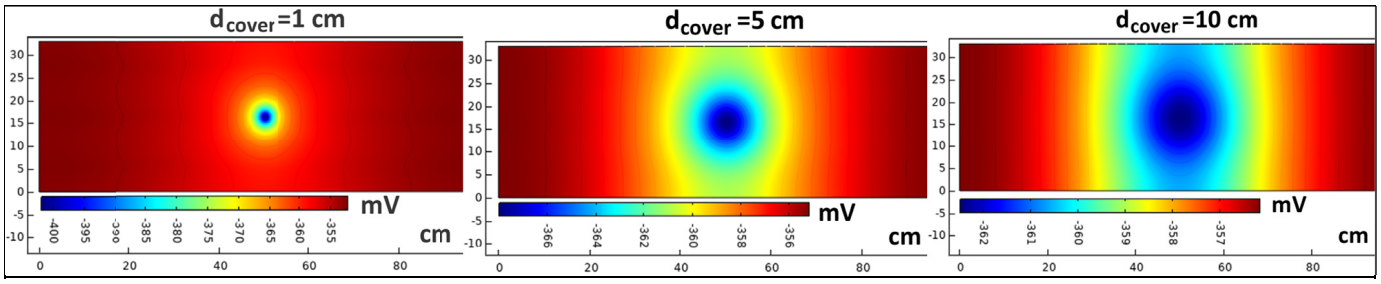

Fig. 7. Two rows of rebars. Electric potential on the top surface of the construction for different thicknesses of the layer. Length of the active site L_{anode} = 0.1 cm. Potential ranges (in mV): [–400, –355] (left panel – 1 cm thickness), [–368, –356] (middle panel – 5 cm thickness), and [–362, –357] (right panel – 10 cm thickness)

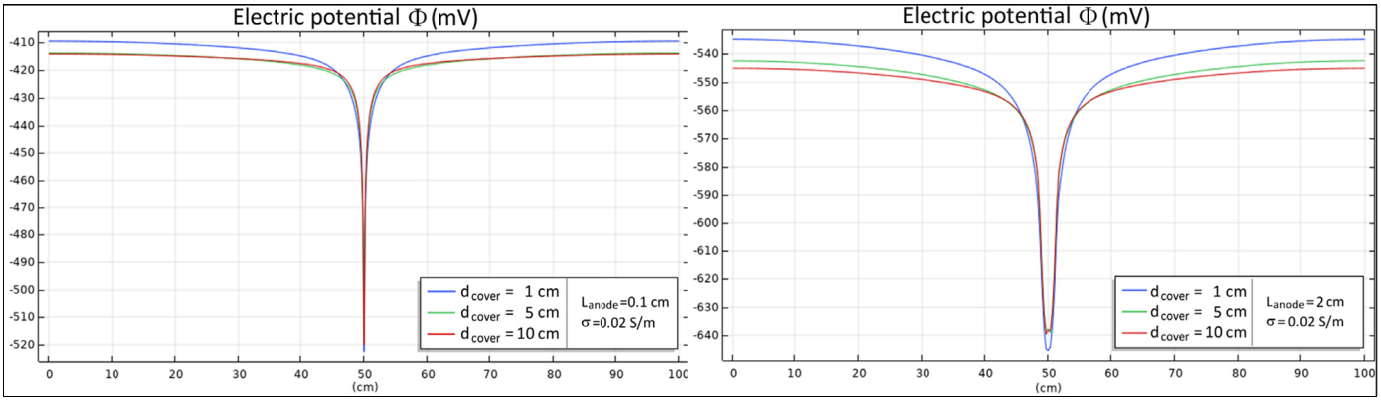

Fig. 8. One row of rebars. Electric potential along the line on the surface of a corroding rebar (with one anodic site). Left panel: length of the anodic site = 0.1 cm; Right panel: length of the anodic site = 2 cm

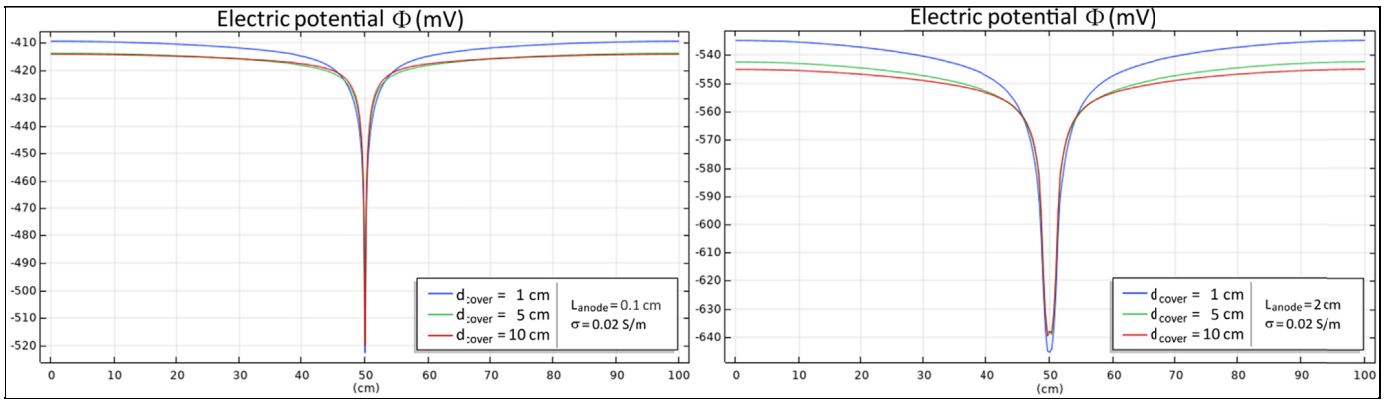

Fig. 9. Two rows of rebars. Electric potential along the line on the surface of the corroding rebar (with one anodic site). Left panel: length of the anodic site = 0.1 cm; Right panel: length of the anodic site = 2 cm

is obvious from these pictures and numerical values of potential, the possibility of detection of these sites through the surface measurement dramatically drops when the concrete layer approaches 5 cm. At this thickness virtually we are not able to find out that there are three sites (the map looks almost the same as with one site).

Finally, we would like to illustrate the impact of the concrete electric conductivity (ionic) on the potential inside the sample. Fig. 12 is an example of such computations for three different values of conductivity.

As can be appreciated the values of the potential strongly depend on the values of conductivity – both greater absolute

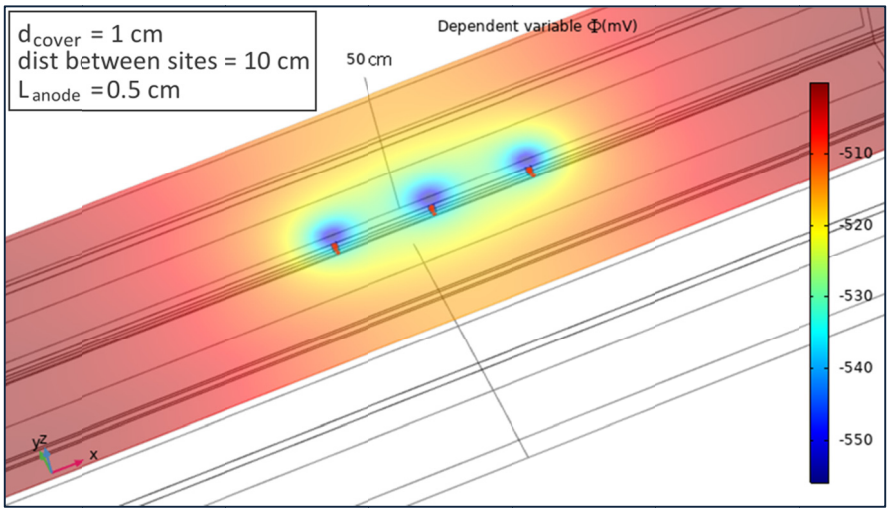

Fig. 10. General view of a corroding rebar embedded in concrete matrix with three anodic sites and electric potential on the top part of the element. Two rows rebars arrangement

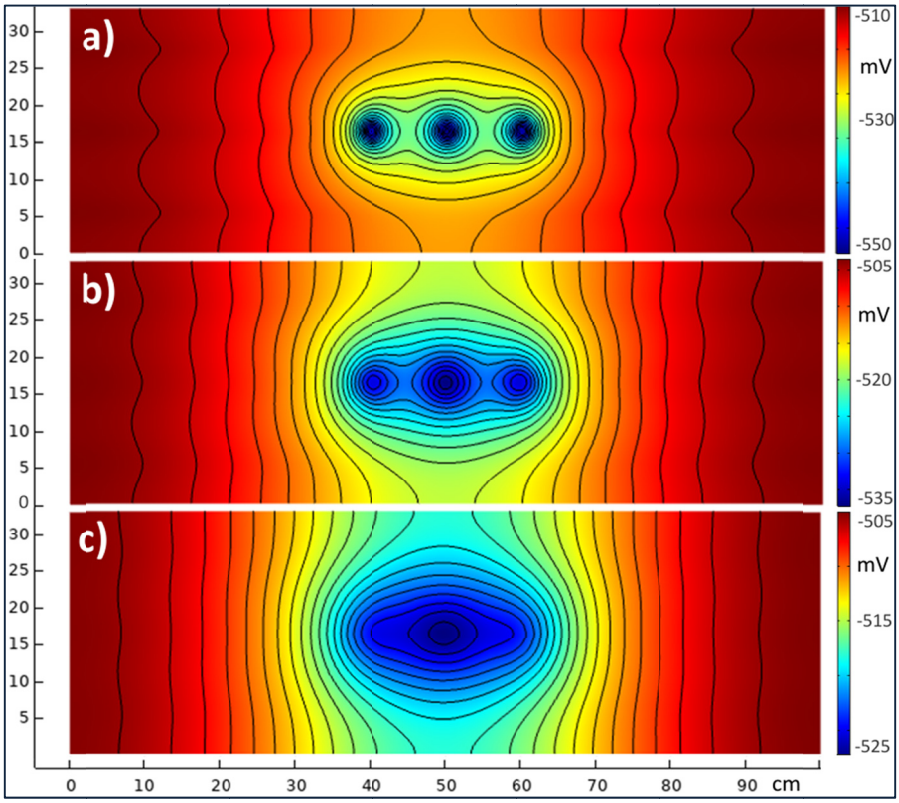

Fig. 11. Dependence of electric current distribution on the top surface in the case of three anodic sites on the concrete layer thickness. In all cases σ = 0.02 S/m, distance between sites = 10 cm, length of anodic site L_{anode} = 0.5 cm. a) d_{cover} = 1 cm; b) d_{cover} = 2.5 cm; c) d_{cover} = 5 cm

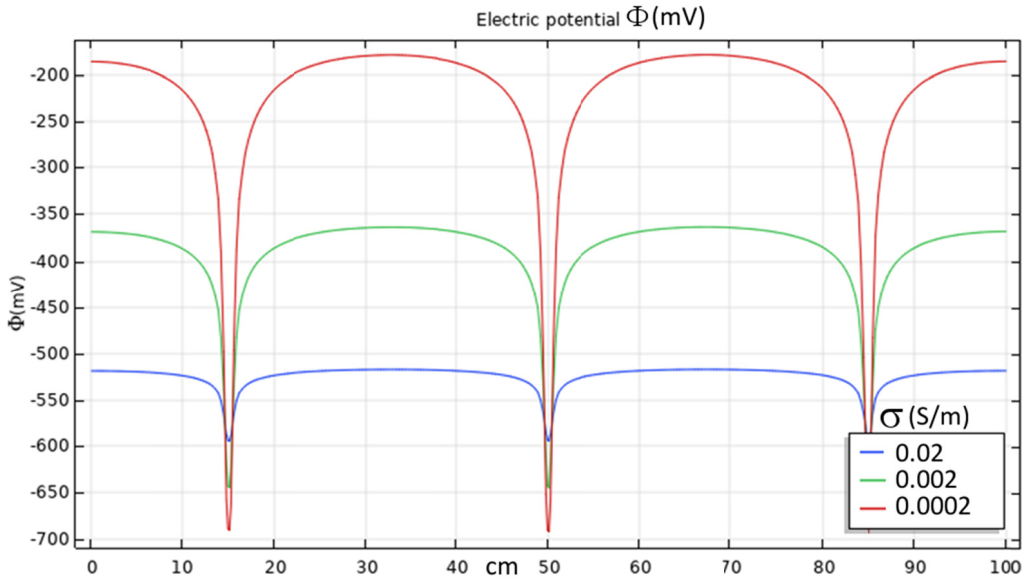

Fig. 12. Electric potential near the surface of the corroding rebar with three active sites

values and gradients are recognized for smaller conductivity (higher resistance). It is important conclusion because the conductivity is not a constant parameter of the concrete sample being strongly dependent on its water content and presence of various ions usually which entered the sample after construction has been built. Thus, without estimation of this state of concrete it is difficult to infer reliable conclusion on the corroding activity from shear potential measurements on the surface.

6. Summary and discussion

In recent years simulations analysis has become common in the corrosion science investigations. Numerical models can function either as predictive tools allowing, for example, a better design of the reinforced structures in order to minimize the detrimental impact of corrosion or as interpretative tools which are especially important in the case of on-site diagnosis of the

corroding state of such structures. Our main goal was to present a computational approach based on the finite element method (FEM) for electrochemical system which models corrosion phenomena in reinforced concrete structures and hint at some possible problems and ambiguities that may arise while using standard tests (e.g., RILEM TC 154-EMC and ASTM C876 – 09) for assessing the corrosion of steel in concrete.

In simulations two types of rebars arrangements have been used (one-row and two-rows) and two types of corroding setting (one active site and three active sites). The influence of concrete layer thickness and concrete on the top potential distribution has been analyzed.

1. The present non-destructive methods of corrosion diagnosis in reinforced concrete constructions are satisfactory with respect to measurement procedures but the interpretations of the results are still ambiguous.
2. Local character of corrosion and complicated geometry of construction buildings require using 3D modeling.
4. Simplification and reduction of 3D models to 2D lead to incorrect interpretation of the in-field measurements (*cf*. Chapter 35 in [1]). The presented analysis shows that currently applied non-destructive methods are only qualitative in nature.
5. Currently available equipment used in on-site measurements, as postulated in the above mentioned norms, is not sensitive enough to reliably assess the corroding activity when the layer thickness is above 5 cm. Moreover, the simulations reveal that the absolute values play a minor role while the variance of the electric potential is more important in localizing the active sites.
7. The nearest future of non-destructive methods of corrosion diagnosis is better interpretation based on better 3D models.
10. The key role will play time-dependent corrosion models taking into account the following aspects: real 3D geometry; concrete microstructure: porosity, cracks; multi-ionic transport (concentrated electrolyte) and chloride binding reactions; oxygen, carbon dioxide and water transport; influence of water on the O_2 and CO_2 transport; variable in time environmental condition (temperature, humidity, winds etc.).
11. Integrating the aforementioned factors into a more comprehensive model will allow a more accurate prediction of the time and locations of corrosion processes.

Acknowledgments

This work was supported by the Polish National Centre for Research and Development Grant No. K1/IN1/25/153217/NCBiR/12, and Grant AGH No. 16.16.160.557.

REFERENCES

[1] S. Laurens, F. Deby, Electrochemical Methods (Chapter 5) in Non-destructive Testing and Evaluation of Civil Engineering Structures, eds. J.P. Balayssac and V. Garnier, ISTE Presss – Elsevier 2018.
[2] J. Ožbolt, G. Balabanić, M. Kušter, Corr. Sci. **53**, 4166-4177 (2011).
[3] S. Laurens et al., Cem. Concr. Res. **79**, 272-290 (2016).
[4] N. Sato, Corr. J. **45** (5), 1989-368 (1989).
[5] B. Elsener, Cem. Concr. Compos. **24**, 65-72 (2002).
[6] G. Qiao, J. Ou, Electrochim. Acta **52**, 8008-8019 (2007).
[7] T.E. Pou, O.J. Murphy, V. Young, J. O'M. Bockris, J. Electrochem. Soc. **131** (6), 1243-1251 (1984).
[8] A. Neville, Mater. Struct. **28**, 63-70 (1995).
[9] V. Cicek, Corrosion Engineering, SP Wiley 2014.
[10] N. Perez, Electrochemistry and Corrosion Science, 2nd ed., Springer (2016).
[11] A.J. Bard, L.R. Faulkner, Electrochemical Methods: Fundamentals and Applications, 2nd ed., Wiley 2001.
[12] A. Quarteroni, Numerical Models for Differential Problems, Springer-Verlag Italia, Milan 2009.